

Evolutionary status and age spread in the young LMC cluster NGC 1850A^{*}

V. Caloi and A. Cassatella

Istituto di Astrofisica Spaziale C.N.R., C.P. 67, I-00044 Frascati, Italy

Received 10 July 1997 / Accepted 1 October 1997

Abstract. *IUE* spectra have been obtained for 15 members of the very young LMC cluster NGC 1850A. The extinction law toward the cluster is similar to the one generally accepted for the 30 Dor region. We derive the effective temperatures and bolometric luminosities to estimate the age and mass for each star. An age spread of 2 to 10 Myr is estimated, suggesting a more or less continuous star formation process. The cluster contains at least four objects with mass $\geq 55 M_{\odot}$, still close to the main sequence. The age of the main cluster NGC 1850 is estimated to be about 50 Myr.

Key words: clusters: globular: NGC 1850A(LMC) – Magellanic Clouds – stars: evolution – UV: stars – galaxies: star clusters

1. Introduction

Populous young clusters allow one to study both the evolutionary patterns of massive stars and the modalities of star formation processes. In particular, time differences in star formation show up easily because stellar evolution proceeds very rapidly here. In preceding papers we investigated NGC 330 in the Small Magellanic Cloud (SMC) and NGC 2004 in the Large Magellanic Cloud (LMC) (Caloi et al. 1993, Caloi & Cassatella 1995). We present now a study of the LMC cluster 1850A, so designated according to Bathia & MacGillivray (1987). The object has been studied recently by Fischer et al. (1993), by Gilmozzi et al. (1994) with the *Hubble Space Telescope* (*HST*), and by Vallenari et al. (1994; see this last paper for a more complete bibliography).

The cluster appears as a subsystem in a rather complex region. It is composed of: a bright clump about 30'' west of the main cluster NGC 1850, bright OB stars as far away as 1' from the clump and a pre-main sequence population, with a spatial extent at least comparable to that of the main cluster (Gilmozzi et al. 1994). It is not yet clear whether it is physically related

to the main cluster NGC 1850 (see the discussion in Vallenari et al. 1994). From past investigations, the system appears very young, with age estimates from 4 to 10 Myr, so it is a good candidate for observing the early evolution of very massive stars and to see whether also its Hertzsprung–Russell (H–R) diagram presents blue giants in rapidly crossed post main sequence gaps (see Grebel et al. 1996 for a review on the subject, but also Hillebrand et al. 1993 for a similar problem in very young clusters).

As in the preceding papers, we shall derive effective temperatures and bolometric luminosities from far UV spectra obtained with the *International Ultraviolet Explorer* (*IUE*) satellite. This time, besides the comparison of spectra with fluxes from LTE model atmospheres, we shall attempt also a spectral classification for a first estimate of the temperature. This procedure turned out to be particularly useful, both because of an intrinsic dispersion in the reddening (Gilmozzi et al. 1994, Vallenari et al. 1994), and because the reddening turned out to be of the 30 Dor type, which shows a weak 2175 Å extinction bump (Fitzpatrick 1985).

The chosen targets cover an interval of three magnitudes (in the visual) and should allow one to explore the region of the unevolved stars. As for the membership, we could not be sure in advance that the faintest targets belonged to the young cluster, but it turned out that the choice we made of objects among the bluest ones at each magnitude secured the desired membership. The only exception is star 3037 in the catalogue by Vallenari et al., that we chose on the “obscured” eastern side of the main cluster (Vallenari et al. 1994), where very few blue stars are observed.

2. Observations and data analysis

We obtained *IUE* low resolution spectra of 15 blue stars in the region of NGC 1850, chosen as explained above. They are listed in Table 1 together with the log of the *IUE* observations, and shown in Fig. 1 on the CM diagram by Vallenari et al. (1994). All the Long Wavelength Primary (LWP) images were heavily contaminated longward of 2500 Å, where the flux distribution exhibits an upturn with solar characteristics, that often saturates the image; we suspect that some contamination is present also at

Send offprint requests to: V. Caloi

^{*} Based on observations collected by the International Ultraviolet Explorer (*IUE*) at the Villafranca Satellite Tracking Station of the European Space Agency.

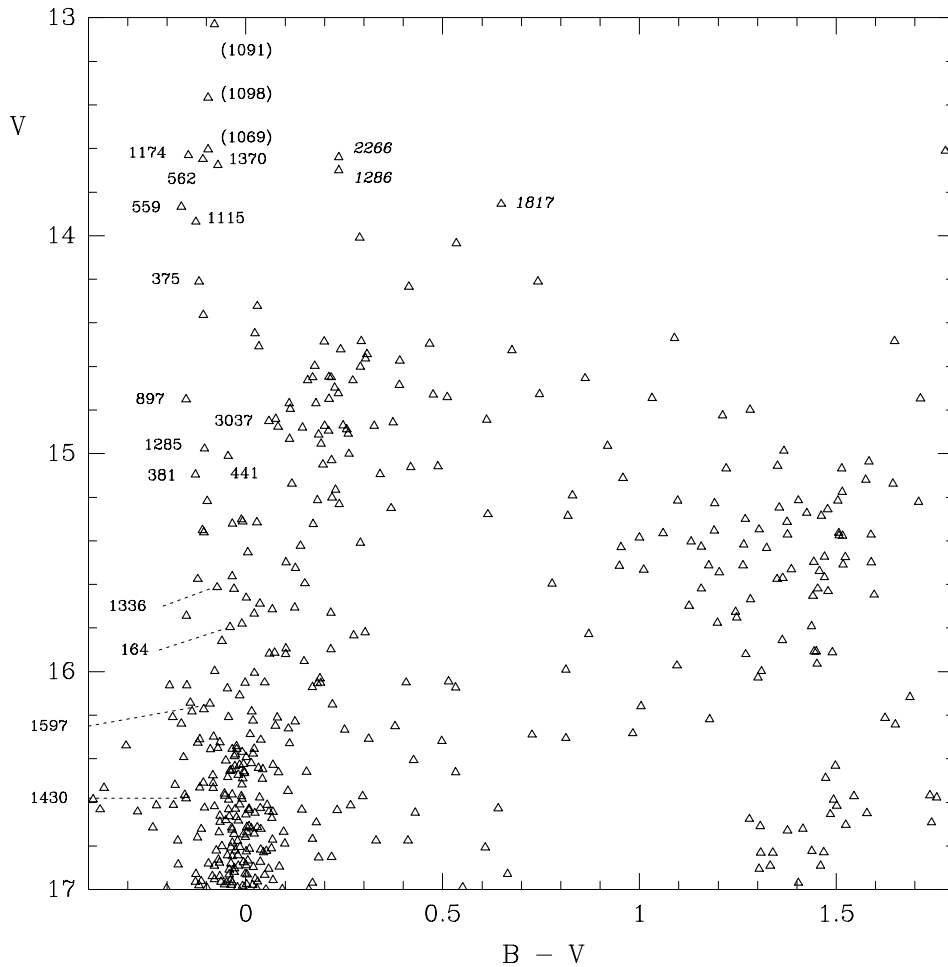


Fig. 1. The program stars on the colour-magnitude (CM) diagram by Vallenari et al. (1994), limited to $V < 17$ mag; in parentheses, the three most luminous stars, not observed with *IUE*, that form with V1115 the central blue knot of NGC 1850A. In italics supposed members of the main cluster in a blue loop phase (see text)

shorter wavelengths. All spectra were processed with *NEWSIPS*, which incorporates the new *IUE* absolute calibrations and takes into proper account the time dependent sensitivity degradation of the *IUE* cameras.

Given the severe crowding problems in the field of the cluster, on six occasions more than one spectrum was found in the $20'' \times 10''$ entrance apertures of the *IUE* spectrographs. In all but one case the contaminating objects are much fainter than the main source (see Fig. 2).

To reconstruct the true energy distribution of the targets in these multiple source exposures we proceeded as in Caloi & Cassatella (1995). The spatially resolved Extended Line-by-Line (ELBL) spectra, once calibrated in flux and averaged over wavelength bands 10 \AA wide, were used to obtain a series of scans perpendicular to the dispersion (cross profiles), corresponding to each of the wavelength bins. A multi-gaussian fit to the cross-profiles was calculated for each multiple exposure, obtaining position, central intensity and FWHM of each resulting gaussian component (the number of the components had to be fixed in advance). A representative sample of the cross profiles obtained and of the corresponding results of the multi-gaussian fits are shown in Fig. 2 for the six multiple exposures examined. We recall that the physical distance between two adjacent scan lines corresponds to half a diagonal pixel on the *IUE* detector

faceplate, or to about $1.08''$ on the sky (Cassatella et al. 1985). The cross profiles shown in the figure refer to the shortest wavelength bands, where the fits were more critical due to the larger noise features; the fits were generally better for $\lambda \geq 1400 \text{ \AA}$. In the following, each multiple image will be briefly discussed.

Star V441

In the Short Wavelength Primary (SWP) image the secondary component appears as a diffuse bump, well separated from the main component. According to Cassatella et al. (1985) two spectra falling in the large aperture may be separated if their distance perpendicular to the dispersion direction is larger than about $4''$: this condition is surely met in the present case. It was necessary to fix the position of the center and the FWHM of the bump to ensure that the resulting gaussian fits gave the main component centered in a fixed position for all wavelength bands, with no interference from the secondary (see Fig. 2a). The FWHM of the main component follows the pattern established by Cassatella et al. (1985), with a minimum around $1300\text{--}1400 \text{ \AA}$. Even the FWHM absolute values follow the predictions, if one takes into account the estimates by Perez et al. (1991), more appropriate to the focus steps (from -4 to -6) of the various time intervals in which the observation has been subdivided (because of the

Table 1. Log of *IUE* observations. Identifications according to Vallenari et al. (1994)

Star	V	R.A.	Dec.	Image	t(min)	Date	Quality
V164	15.795	050842	-684859	SWP56841	550	210296	503
V375	14.210	050845	-684906	SWP56284	72	111295	400
V375	14.210	050845	-684906	LWP31812	63	111295	501
V381	15.095	050845	-684923	SWP56277	150	081295	500
V381	15.095	050845	-684923	LWP31805	120	081295	501
V441	15.011	050846	-684832	SWP56843	288	220296	501
V441	15.011	050846	-684832	LWP32017	216	220296	801
V559	13.867	050848	-684911	SWP56280	40	111295	400
V559	13.867	050848	-684911	LWP31808	40	111295	501
V562	13.649	050848	-685015	SWP56281	45	111295	500
V562	13.649	050848	-685015	LWP31809	36	111295	501
V897	14.751	050852	-684931	SWP56837	81	200296	500
V897	14.751	050852	-684931	LWP32010	81	200296	502
V1115	13.936	050854	-684933	SWP56276	50	081295	600
V1115	13.936	050854	-684933	LWP31804	45	081295	600
V1174	13.631	050854	-684908	SWP56282	32	111295	400
V1174	13.631	050854	-684908	LWP31810	31	111295	501
V1285	14.977	050855	-684828	SWP56285	110	111295	400
V1285	14.977	050855	-684828	LWP31829	135	171295	501
V1336	15.613	050856	-685045	SWP56863	120	280296	300
V1370	13.676	050856	-685011	SWP56283	68	111295	500
V1370	13.676	050856	-685011	LWP31811	34	111295	501
V1430	16.582	050858	-684838	SWP56279	325	101295	401
V1430	16.582	050858	-684838	LWP31815	335	121295	703
V1597	16.146	050857	-684805	SWP56295	478	141295	303
V3037	14.851	050914	-684916	SWP56849	550	240296	303

well known problems in the last period of *IUE* operations). At the same time, bad bins are present, with poor fits, in heavily disturbed spectral regions. As for the LWP image, it was not necessary to fix any parameter to obtain good fits; the spectrum was cut at 2500 Å, as in all other images, owing to the contamination by the solar spectrum. The resulting extracted spectrum is shown in Fig. 3a: a few spectral features are recognizable and the overall behaviour compares well with Kurucz fluxes from model atmospheres (see later).

Star V897

Two sources are visible in the cross profile of Fig. 2b, the stronger corresponding to V897. The neat separation allows to obtain a good fit of the cross profiles without fixing any parameter, with the FWHM following closely the expected behaviour, as for V441. The extracted spectrum is shown in Fig. 3d.

Star V1115

The SWP cross profiles show a central peak (the target) plus two small diffuse bumps on the wings (Fig. 2c). The gaussian fits obtained fixing the positions of the secondaries are satisfactory, with the FWHM of the target marginally higher than found for V441 and V897 (the focus being marginally higher, about – 4). In the LWP cross profiles, the bump at the left disappeared, and the deconvolution algorithm required to fix the FWHM of the

remaining secondary to obtain good fits with no perturbation on the primary. However, the comparison with theoretical spectral distributions showed an inconsistency in the flux level (Fig. 3c), that we ascribed to the strong background, since the star belongs to the small group of hot stars at the center of the subcluster under investigation (see Fig. 7b).

Star V1336

Only the SWP image was obtained. The situation is similar to that found for V1115, with one central peak (the target) plus two small bumps on the wings. The image quality is lower than in the preceding cases. We had to fix both center and FWHM of the secondary components to obtain good fits (Fig. 2d). Fits to the main component approximate the expected FWHM quite well and yield a well defined central value, although at all wavelengths the absolute value is always higher than predicted theoretically (about 20% considering data from Perez et al. 1991). Since spectral noise, background noise and drift in the satellite configuration may broaden the ideal point-spread function, we consider the fits obtained to be satisfactory. The extracted spectrum is shown in Fig. 3b.

Star V1430

Only the SWP image was obtained. Same configuration in the slit as for V1115 and V1336 (Fig. 2e); both center and FWHM

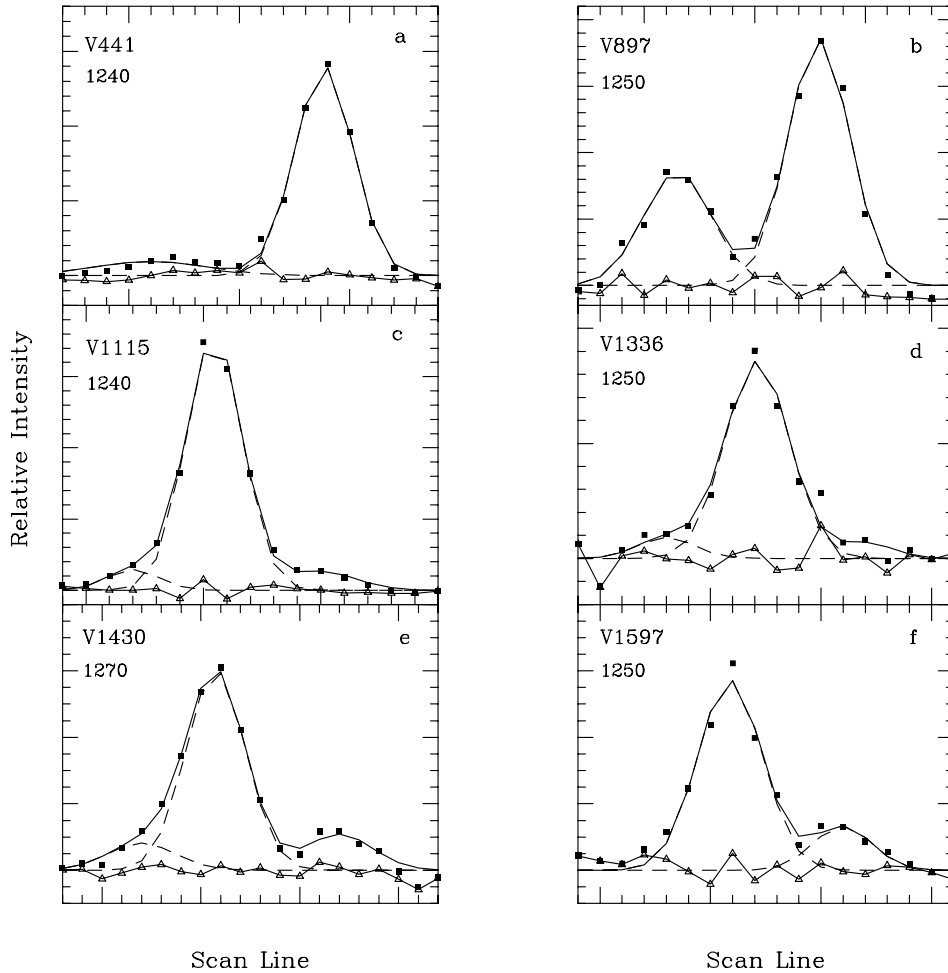


Fig. 2a–f. A sample of the cross profiles (filled squares) and of the corresponding gaussian fits (full line: total, dashed line: individual components, open triangles: residuals). The centers of the 10 Å wavelength bands over which the ELBL has been averaged are indicated. Each tick on the abscissae indicates one scan line

of the secondaries were fixed. The spectrum is often noisy, so that the cross profiles are sometimes less satisfactory than the one shown in Fig. 2e. The FWHM of the primary follows on the average the expected behaviour, but with more irregularities than found for V1336, and a stronger increase at $\lambda \geq 1600$ Å. The extracted spectrum is given in Fig. 3e.

Star V1597

Only the SWP image was obtained. Two components in the aperture, well separated. The deconvolution without fixed parameters gives satisfactory fits to the cross profiles (Fig. 2f), with a well behaved FWHM, only slightly larger than the one found for V441 and V897. The extracted spectrum is shown in Fig. 3f.

The single source spectra were obtained through the standard *IUE* extraction software.

3. Stellar temperatures

3.1. The metal content

The direct determinations of the metallicity of NGC 1850 give values from $Z = 0.004$ (Grebel et al. 1992, based on Stroemgren photometry of five stars), to 0.009 (Schommer & Geisler 1988,

based on Washington photometry of three stars) and to 0.014 (Jasniewicz & Thevenin 1994, from medium resolution spectra of two stars). The discrepancies among these measurements, the uncertainties in the various methods and the small number of stars examined do not allow one to make a safe choice of the cluster metallicity from observations of cluster members. So we chose to adopt the average metal abundance of the LMC, generally given at about one third solar (see, e.g., Russell & Bessell 1989 and Russell & Dopita 1990), and to use Kurucz (1993) model atmospheres with $[\text{Fe}/\text{H}] = -0.5$ ($Z \simeq 0.006$) for comparison with *IUE* fluxes. The adopted Z is not critical for this comparison, since the results change only marginally using Kurucz models with solar composition. The relevance of the uncertainty on Z for the comparison with stellar evolution predictions will be discussed in Sect. 4.

3.2. The reddening

An accurate reddening correction of the observed energy distribution is necessary to obtain a reliable estimate of stellar temperatures by comparison with Kurucz models. However, as already mentioned, the region of NGC 1850 presents an intrinsic dispersion of the reddening. Vallenari et al. (1994) suggest that, from the large scatter of the data, a differential reddening of 0.1

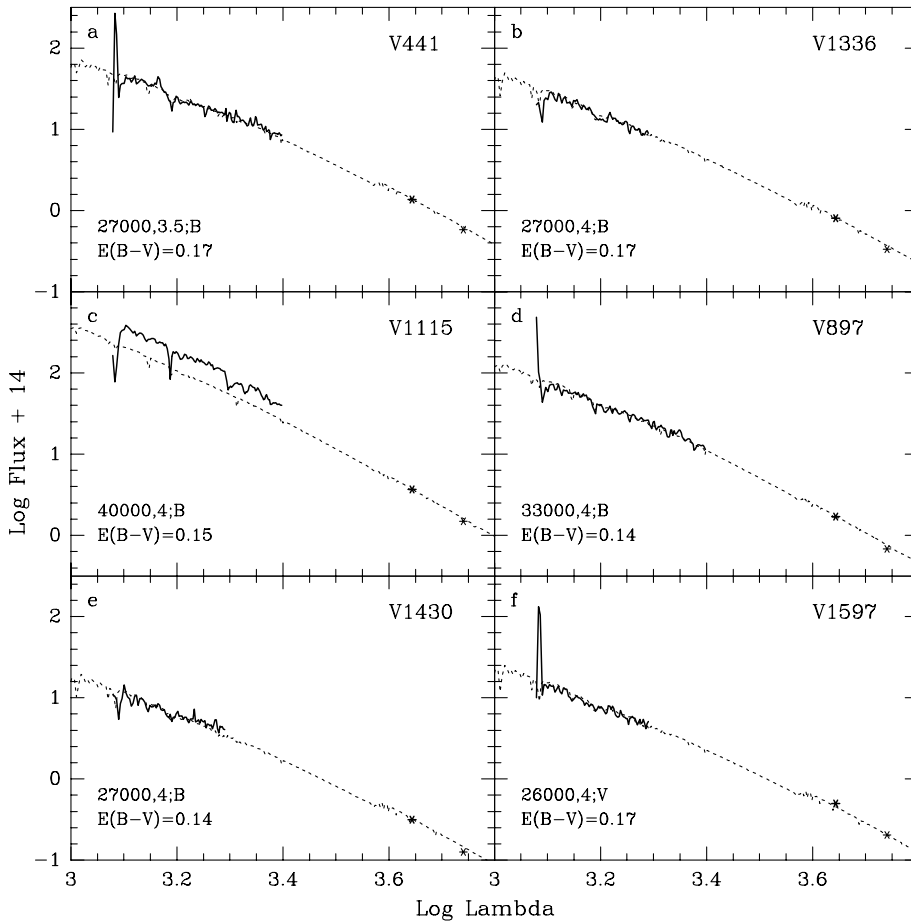


Fig. 3a-f. Flux distribution from gaussian fits for all the multiple spectra, plus the chosen fits with Kurucz model fluxes. For each Kurucz model T_{eff} , $\log g$, zero point for scaling (F_B or F_V , indicated by asterisks) and adopted total reddening are given. The heavy element content is always $[\text{Fe}/\text{H}] = -0.5$

mag may be present. Gilmozzi et al. (1994), through *HST* observations, estimate an average reddening $E(B - V) = 0.18 \pm 0.02$, but found evidence for fluctuations in the extinction from star to star of the order of $\Delta E(B - V) = \pm 0.04$.

The occurrence of a variable reddening introduces some complications in the process of temperature estimate, since it is no longer possible to derive a standard value of $E(B - V)$ from integrated spectra and from a suitable selection of the best quality spectra, and then to apply it safely to all the other objects.

The estimate of the reddening contributions from the Galaxy and from the LMC was the result of trials and iterations. We started with a value of 0.04 mag for the galactic foreground reddening (Nandy et al. 1979). Then we made extensive tests with two reddening laws for the LMC, that is, the one by Fitzpatrick (1986) generally accepted for the main body of the LMC, which follows a law with wavelength similar to that of the Galaxy, and the one by Fitzpatrick (1985) more specific for the region of 30 Dor, which shows a weak 2175 Å extinction bump and a steep far ultraviolet increase. This latter law was found appropriate for other young star systems (Wilcots et al. 1996, Will et al. 1996).

It was immediately evident from the first comparisons between Kurucz (1993) models and stellar *IUE* fluxes that the 30 Dor law gave the best approximation to the desired reddening corrections. In fact, all the fits with the average LMC law showed

a clear flux deficit towards the shortest wavelengths, which could not be compensated for by an increase in the extinction internal to the LMC, without giving rise to an abnormal flux increase at the 2175 Å extinction bump. When using the 30 Dor reddening law, it turned out to be much easier to reach an acceptable fit with Kurucz theoretical distributions, since this law gives a far ultraviolet extinction much steeper than the average LMC law.

At this point, we checked the reliability of the assumption on the galactic foreground. Unfortunately, NGC 1850 lies outside the region for which Oestreicher et al. (1995) give a detailed map of the reddening distribution in the foreground of the LMC, and a similar map by Schwering and Israel (1991) is not detailed enough for our purpose. On the whole, these investigations as well as preceding ones (see Bessell 1991 for a review), suggest a larger value for the galactic foreground reddening than that by Nandy et al. (1979). So we repeated the trials with the two reddening laws for the LMC, adopting values larger than 0.04 mag for the galactic contribution to the reddening.

Again the 30 Dor law turned out to be more appropriate, but the fits with Kurucz models required much higher T_{eff} than before and were less satisfactory. For example, with a galactic foreground of 0.08 mag, the fitting T_{eff} for V1285 increased from 30000 K to 37000 K (total $E(B - V) = 0.18$). A foreground of 0.06 mag gives results not too different from those found with 0.04 mag (total $E(B - V) = 0.14$), but the fits are worse.

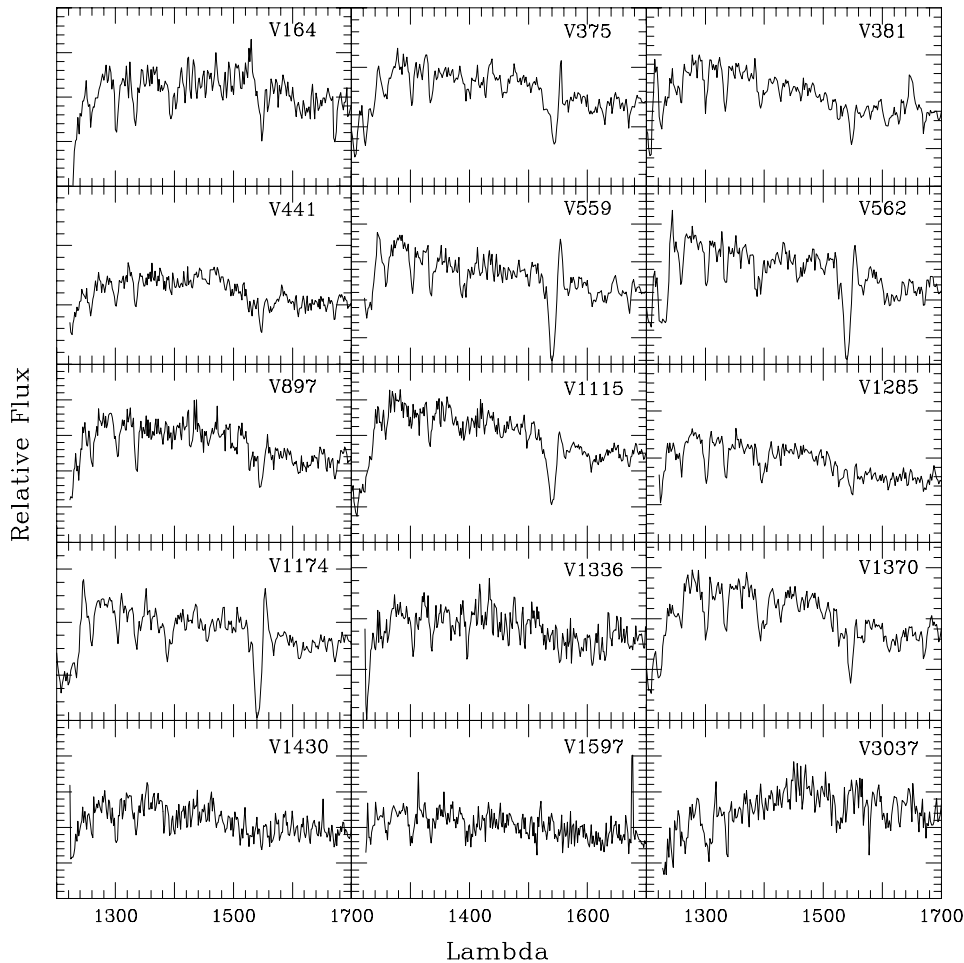


Fig. 4. The spectral region from 1200 to 1700 Å is shown for all the program stars; for multiple images, the EBLB lines at the intensity peak of the target have been used. Ordinate: flux in relative units.

The final choice took into account the constraints on T_{eff} by spectral classification, as we shall see in the following subsections. The consistency with the indications from spectral types requires clearly effective temperatures of the order of those obtained with a foreground galactic reddening of about 0.04 mag. The fact that the fits with Kurucz models appear definitively better using this value for the foreground than with a larger one supports such a conclusion.

3.3. Spectral classification

To have an independent estimate of the T_{eff} of the targets without making any assumption on the reddening, we attempted a spectral classification using the C IV 1550 Å and the Si IV 1400 Å doublets, which are generally strong in our spectra (see Fig. 4). The presence in about one third of the spectra of a P Cyg profile in the C IV line improves the chances of discriminating among O spectral types, according to the strength of both absorption and emission intensities.

The equivalent widths W_{λ} of the C IV and Si IV lines were measured in about 40 standard stars taken from the *IUE* Low Dispersion Spectra Reference Catalog (Heck et al. 1984) to obtain the behaviour of W_{λ} 's versus spectral type, for spectral types from O5 to A3, and for luminosity classes V and III. In spite of the limitations imposed by the use of low resolution

data, we found that, on average, the relationships were consistent with the results by Walborn & Panek for O stars (1984) and by Rountree & Sonneborn (1991) for B stars. We estimate that an accuracy of one spectral subclass can be achieved, at least in the most favorable cases.

For the luminosity class V we found the following criteria:

- Si IV absorption line at 1400 Å: maximum at B1, disappears at O6 and B6.
- C IV absorption line at 1550 Å: intensity declines from early O types and disappears at B2.
- C IV emission line at 1550 Å: strong until O6, decreases in O7 and disappears at O9.

In order to classify our targets, first of all we gave a tentative classification of the luminosity class on the basis of M_V , following the prescriptions by Vacca et al. (1996). Possible ambiguities (same M_V , different luminosity class) are avoided on the basis of the large difference in T_{eff} involved: e.g., a star with $M_V = -5.3$ has a T_{eff} of about 45000 K if it belongs to class V, and of 30000 K if it belongs to class III. The spectral type and the fits with Kurucz models allow to make a safe choice, even taking into account a range of galactic foreground reddenings.

All the stars belong to luminosity class V, except for V1370 (luminosity class III) and V3037 (will be discussed separately).

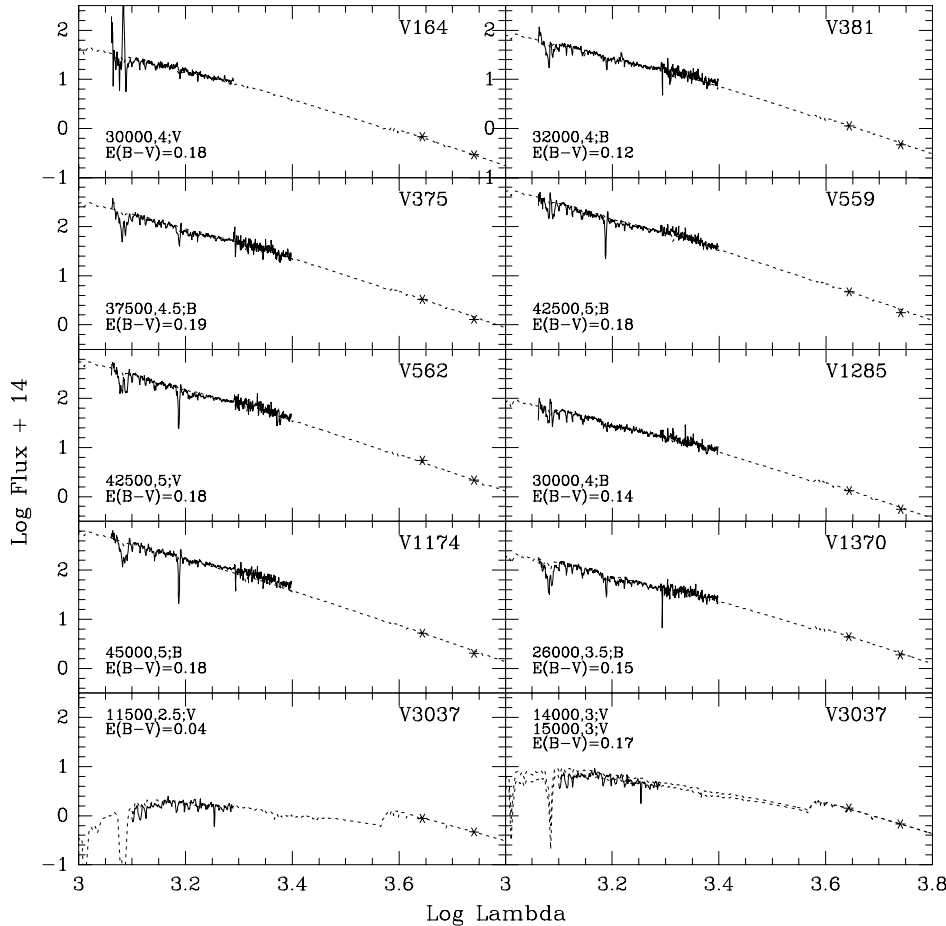


Fig. 5. As in Fig. 3, for the single source spectra.

Then we measured the C_{IV} and Si_{IV} lines with the same method used for the standard stars. In the case of multiple exposures, the equivalent widths were measured after re-extracting the spectra from the ELBL, using only three scan lines at the intensity peak of the target. Though this spectrum does not reproduce the true flux distribution with wavelength, it still provides the main features of the target spectrum (the contribution by the secondaries to the spectral line intensities of the primary targets may be safely considered as negligible).

In Table 2 the adopted spectral classification is reported. The final choice was a compromise among the indications given by the W_λ 's of interest, with a strong weight given to the presence and the intensity of the C_{IV} emission. For the faintest stars (V164, V1336, V1430 and V1597), it was not possible to obtain reliable W_λ 's because of the noise; the indicated spectral types (in parentheses) were derived from qualitative estimates and from the fits with Kurucz models.

In star V441 (multiple exposure spectrum) the Si_{IV} absorption line (almost absent) is definitely fainter than expected from the spectral type (about B1 V) deduced from the presence of a weak, but clear C_{IV} absorption line. The discrepancy is likely due to spectral noise and we considered the information provided by the C_{IV} line to be more reliable.

In contrast, in the hottest objects – V1174, V562, V559 – the Si_{IV} 1400 Å line is definitely stronger than expected from the spectral type deduced from the C_{IV} P Cyg profile and a

luminosity class V. Such higher strength is likely due to a luminosity intermediate between classes V and III, class III spectra showing no correlation between Si_{IV} W_λ and the specific O spectral type. As a matter of fact, the M_V 's of the quoted stars are somewhat lower than expected for class V objects, even if clearly far from class III values (see Table 2 and Vacca et al. 1996, Table 5).

The coolest spectrum is apparently that of V3037, the only star observed east of the main cluster center. Only the SWP exposure was obtained. The spectrum is noisy, but the C_{IV} and Si_{IV} lines are surely absent (Fig. 4), which indicates a type later than B5 (Rountree and Sonneborn 1991). The intensities of the lines at 1300–1310 Å, of Si_{II} at 1530 Å and of Al_{II} at 1860 Å, point to the same direction. On the other hand, the type cannot be later than B9 from the shape of the continuum towards Ly α (compare with the IUE Low Dispersion Spectra Reference Atlas (Heck et al. 1984) and the IUE Ultraviolet Spectral Atlas (Wu et al. 1983)). Therefore, from M_V (not higher than -3.65 mag) the luminosity class is at least III. The final choice of the spectral type will be discussed together with the fits with Kurucz models.

3.4. Fits with Kurucz models

Having obtained an indicative range of temperatures for each star, we proceeded with the (final) comparison of each IUE spectrum with the theoretical flux distributions corresponding to the

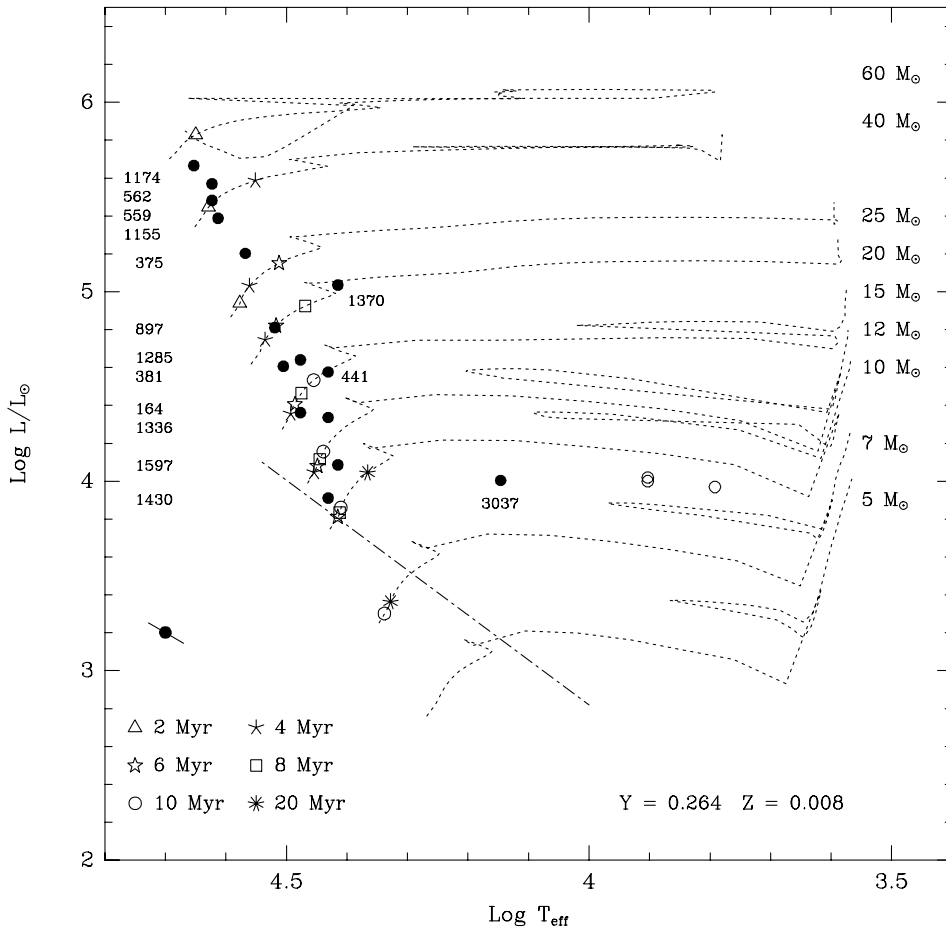


Fig. 6. The program stars (dots) on the theoretical HR diagram, together with evolutionary tracks by Schaerer et al.; open circles indicate the supposed main cluster members in a blue loop phase. On the left, the average error bars corresponding to an uncertainty in T_{eff} of 2000 K. The dash-dotted line gives the observational limit of present investigation. On the tracks a few selected ages are indicated.

suggested T_{eff} 's. When consistency is found with the estimates from spectral classification, the indicated temperature will be accepted as the correct one. Also the reddening of each star is estimated in this way. We shall illustrate the procedure in the following.

As mentioned before, the adoption of a galactic foreground larger than $0.04 \div 0.06$ mag gives T_{eff} 's largely inconsistent with the indications from spectral types. This a consequence of the fact that the fitting procedure requires a substantial contribution from the steep 30 Dor law, and that the galactic foreground gives a sort of zero level to which the LMC reddening is added. The higher this level, the higher the required fitting T_{eff} . On the basis of the quality of the fits, our best guess for the foreground reddening is 0.04 mag.

Most of the present targets are very hot stars, and *IUE* spectra give the Rayleigh–Jeans tail of their spectral distributions. Therefore, the temperatures derived through a comparison with theoretical models are in principle rather sensitive to the chosen zero point for the scaling.

We tried both B and V magnitudes as zero points, and found always very little discrepancies among these and either F_V or F_B . Whenever such small differences appeared important, we chose the zero point that resulted in the best fit, since it is the goal of this analysis to obtain a consistent fit within the observational constraints.

As for the reliability of the photometry, we compared the values of V and $(B - V)$ for four blue luminous stars from Vallenari et al. (1994) with corresponding values from Fischer et al. (1993): the $(B - V)$'s are identical within the photometric errors and the V magnitudes differ of few hundredths of a magnitude; so the use of Vallenari et al.'s photometric data should not introduce any relevant uncertainty on the fits.

A short discussion on the fits will be given in the following. As previously stated, we adopt a foreground galactic reddening of 0.04 mag, the 30 Dor law is adopted for the LMC reddening and all stars, except for V1370 and V3037 (luminosity class III), belong to luminosity class V.

Bright stars: $V \leq 15.5$ mag

As an example, we consider in detail V1174. The star temperature has to be higher than 40000 K, given the strong emission in the CIV line; this requires an LMC reddening of at least 0.13 mag.

F_B was chosen as zero point for the fit; from Fig. 5 it appears evident that the discrepancy with F_V (of the order of 2%) may easily be attributed to residual photometric uncertainties (see also later).

In the same figure, the LWP signal appears higher than the corresponding theoretical flux, an occurrence found in almost

all the fits. As already mentioned (Sect. 2), we suspect that the contamination by solar radiation in LWP images may affect the flux level all along the dispersion in wavelength and not only beyond 2500 Å, where it clearly dominates.

We tried fits with Kurucz models with $T_{\text{eff}} = 42500$ K and 45000 K, and $\log g = 5$ (the only available value). The values of the local (LMC) $E(B - V)$ turned out to be 0.13 and 0.14 mag, respectively. In the wavelength range we are dealing with, it is impossible to distinguish between the flux distributions quoted above: we chose 45000 K as T_{eff} for V1174 trusting the spectral classification given before and following the temperature calibration for O stars given by Vacca et al. (1996).

To check a little further the uncertainties involved in the procedure, we considered the F_V and F_B fluxes derived from Fischer et al.'s photometry (star 127 = V1174, $V = 13.69$, $(B - V) = -0.14$). The discrepancy between the zero points is halved, and the fit with Kurucz model with $T_{\text{eff}} = 45000$ K is obtained with an LMC reddening of 0.12 instead of 0.14. Therefore the preceding estimates for T_{eff} and $E(B - V)$ appear confirmed within the uncertainties; we shall adopt the reddening values derived from the photometry by Vallenari et al. for consistency with all other temperature evaluations.

Our estimate of the uncertainty on T_{eff} is of about ± 2000 K, taking into account the uncertainties in spectral type and on the fits with Kurucz models, which involves the choice of the reddening value. As for the reddening itself, the very steep dependence on wavelength of the 30 Dor law defines very precisely (at least formally) the required amount, so that its uncertainty is mainly caused by spectral noise and photometric errors. We estimate the uncertainty to be of the order of ± 0.03 .

For the other spectra – single and multiple sources – we followed a similar procedure, checking that a temperature of the order of the one derived from the spectral type gave a consistent fitting with the corresponding Kurucz model. Such a fit was always possible for single source spectra and four of the multiple source ones, being generally the best fit obtained with a temperature very close to the one indicated by the spectral classification. The implied total reddenings (see Table 2) lie in the range 0.15 ± 0.04 . The results of the fitting procedures are shown in Figs. 3 and 5.

Faint stars: $V \geq 15.5$

For the faint stars (V164, V1336, V1430 and V1597) the fits were performed with a $E(B - V)$ in the interval found for the brighter objects, taking into account the constraints, admittedly weak, given by the CIV and SiIV lines. An error of ± 2000 K is estimated.

In all the trials, the flux distribution of V1430 exhibits a progressive increase with wavelength above the expected theoretical distribution (see Fig. 3e). This occurrence is likely related to the difficulty encountered in the cross profiles fit (see Sect. 2), when an unexpected increase in the FWHM was found for $\lambda \geq 1600$ Å.

Star V1115

We already mentioned that the whole *IUE* spectrum of this object appears abnormally enhanced (Fig. 3c); a strong stellar background due to the position of the object in the cluster (Fig. 7b) appears as a convincing explanation. Therefore we estimated the T_{eff} exclusively on the basis of the spectral classification.

Star V3037

The spectrum appears deformed around 1400 Å, with the presence of a sort of bump (Fig. 4). With a total reddening of the order of the average 0.17, we estimate $T_{\text{eff}} \sim 14000$ K (spectral type about B6; Fig. 5). Higher reddenings would give higher temperatures, but the spectrum described in Sect. 3.3 seems not to allow $T_{\text{eff}} > 15000$ K.

If the star belongs to the LMC field, it could have a lower T_{eff} , down to about 11000 K (spectral type about B9), supposing that only the foreground galactic reddening of 0.04 mag is present (Fig. 5). Another possibility is that the star belongs to the Galaxy, in which case it would be consistent with being a halo field blue horizontal branch object.

3.5. Luminosities, gravities and masses

From the adopted values of the effective temperatures and from the observed V magnitudes, stellar bolometric luminosities have been determined using Kurucz bolometric corrections (1993). We adopted $A_V/E(B - V) = 3.1$, $M_V(\odot) = 4.80$ and a true distance modulus of 18.50 mag (Panagia et al. 1991). The larger modulus of about 18.60 mag suggested by recent estimates based on *Hipparcos* data (Feast & Catchpole 1997, van Leeuwen et al. 1997) would give slightly more luminous structures, with no substantial influence on the results.

We derived the luminosities also from the star radii, that is, from the relation:

$$R^2 \pi F_\lambda = d^2 f_\lambda$$

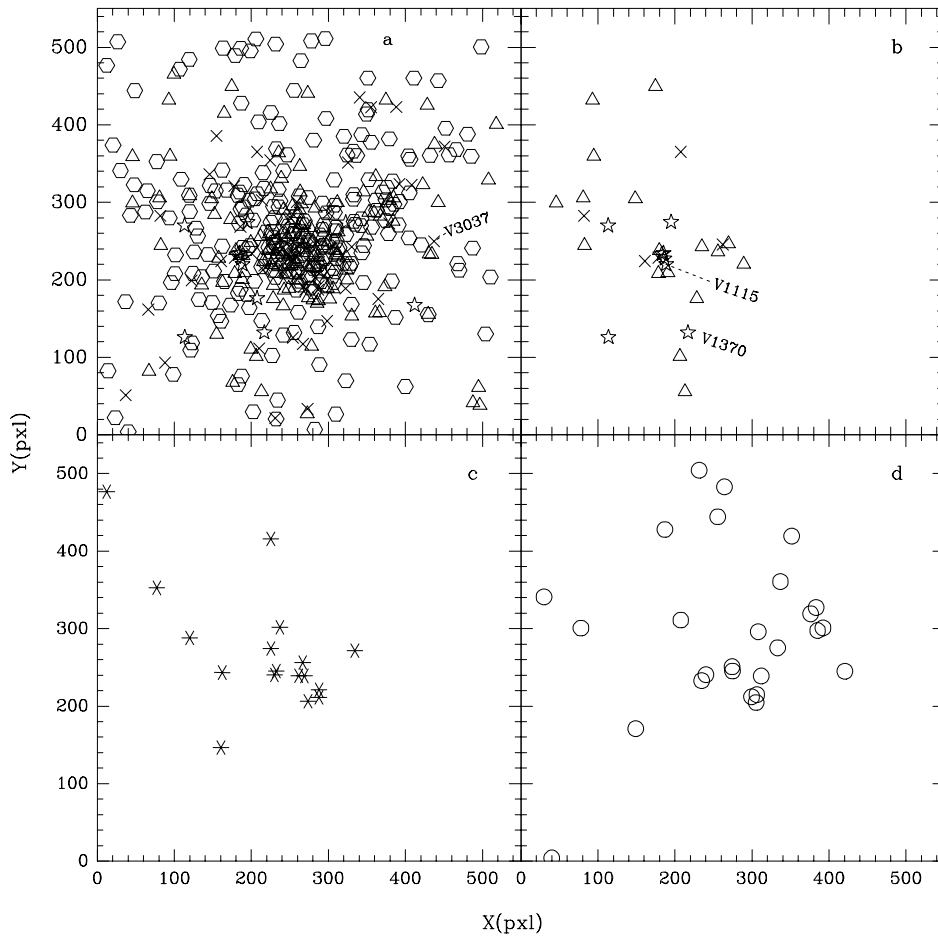
where R is the stellar radius, πF_λ is the physical flux at the star surface, d the distance and f_λ the measured flux at the Earth. Since the flux emitted by the star is taken from the same (Kurucz) models from which the B.C.'s are derived, the two estimates are not independent. Nevertheless, the results may tell something on the overall consistency of the estimates of the various stellar parameters. The visual fluxes were taken as scaling factors. The luminosities turned out very close to those determined from B.C.'s, as expected.

Gravities and masses

UV fluxes are not very sensitive to gravity; we checked that the order of magnitude of $\log g$ required by the Kurucz fits were consistent with the evolutionary mass implied by the inferred temperature and bolometric luminosity, and obtained the estimates in Table 2 for $\log g$ and stellar mass. The overall self-consistency is quite good.

Table 2. Photometric data, colour excess, temperatures and luminosities for the program stars. Approximate spectral types (luminosity class V unless indicated) and estimates for gravities and masses (in solar units) are also given. Identifications as in Table 1.

Star	V	$(B - V)$	Sp.Type	$E(B - V)$	T_{eff}	$\text{Log } L/L_{\odot}$	$\log g$	M_{star}
V164	15.80	-0.04	(B0.5)	0.18	30000	4.36	≥ 4	14
V375	14.21	-0.12	O8	0.19	37000	5.20	≤ 4	27
V381	15.10	-0.13	B0	0.13	32000	4.60	≈ 4	17
V441	15.01	-0.05	B1	0.17	27000	4.57	≈ 3.7	15
V559	13.87	-0.16	O6.5	0.18	42000	5.48	≈ 4	40
V562	13.65	-0.11	O6.5	0.18	42000	5.57	≈ 4	45
V897	14.75	-0.15	B0	0.14	33000	4.81	≤ 4	20
V1115	13.94	-0.13	O7	0.15	41000	5.38	≈ 4	35
V1174	13.63	-0.15	O5.5	0.18	45000	5.66	≈ 4	55
V1285	14.98	-0.11	B0.5	0.14	30000	4.64	≤ 4	16
V1336	15.61	-0.07	(B0.5-B1)	0.17	27000	4.33	≤ 4	13
V1370	13.68	-0.07	B0.5-B1 III	0.15	26000	5.03	≤ 3.5	20
V1430	16.58	-0.15	(B1)	0.14	27000	3.91	≥ 4	10
V1597	16.15	-0.09	(B1)	0.17	26000	4.08	≈ 4	11
V3037	14.85	+0.06	(B6)	0.17	14000	4.00	≤ 3	8

**Fig. 7.** **a** space distribution of all the stars measured by Vallenari et al. ($V < 17$) in the field of NGC 1850; stars: $13 < V < 14$; crosses: $14 < V < 15$; open triangles: $15 < V < 16$; exagons: $16 < V < 17$. **b** space distribution of stars with $(B - V) < 0$ and $13 < V < 16$. **c** space distribution of stars with $(B - V) < 0$ and $16 < V < 16.3$. **d** space distribution of stars with $(B - V) < 0$ and $16.3 < V < 16.5$ (pixel size: $0.46''$).

4. Evolutionary status and age spread

4.1. The theoretical H–R diagram

The location of the program stars in the theoretical H–R diagram is shown in Fig. 6, together with the evolutionary tracks by Schaerer et al. (1993, obtained from the Centre de Données Stellaires at Strasbourg), for a heavy element content $Z = 0.008$, close to the LMC composition discussed in Sect. 3.1; the tracks are for non rotating single stars.

Points with the same age are shown on the tracks for ages from 2 to 20 Myr. The H–R diagram in Fig. 6 indicates that stars up to about $50 M_{\odot}$ are found in NGC 1850A and that an age spread of about 10 Myr is present, at least for stars from 10 to $50 M_{\odot}$. This estimate is based mainly on V1370, a star which, on the basis of M_V as well as of the derived H–R location and gravity, is certainly a giant. Stars of lower luminosity would indicate a higher spread, but for them the uncertainties associated with the quality of the spectra (crowding in the field, spectral noise) somewhat weaken the conclusion.

It is interesting that the most massive stars (V1174, V562, V559 and V1115) appear to be the youngest ones, with an age of about 2 Myr; a similar result was found by Wilcots et al. (1996) for the LMC clusters NGC 2014 and NGC 1770. However, considering the uncertainties, also other luminous stars, such as V375, V897 and V381, might be considered coeval with the brightest ones. The presence of an evolved giant (V1370) with mass lower than the one of the stars at the main sequence tip, is a common feature in many young clusters and associations (see Hillebrand et al. 1993).

In order to check the influence of the chosen Z on age estimate, we compared the evolutionary tracks by Schaerer et al. (1993; $Y = 0.264$, $Z = 0.008$, overshooting parameter $d/H_p = 0.20$) with the ones by Charbonnel et al. (1993; $Y = 0.252$, $Z = 0.004$, overshooting parameter $d/H_p = 0.20$). The differences for what concerns the hydrogen burning phase are negligible. The $15 M_{\odot}$ model with the higher Z exhibits a blue loop, while the model with the lower value ignites helium at $T_{\text{eff}} \sim 4.1$, but since the cluster under investigation has no red or blue loop giants, this occurrence has no influence on our conclusions. Keeping in mind also the result by Cassisi et al. (1994), who showed that moderate variations in star metallicity or original helium content do not affect sensibly the expected H–R diagrams for galactic clusters, we may safely assume that present conclusions are largely independent of the choice of the assumed Z for the comparison isochrones.

We checked also the influence of different treatments of overshooting and convection on the results. We compared the evolutionary track for $20 M_{\odot}$ by Schaerer et al. with the one by Brocato & Castellani (1993; $Y = 0.27$, $Z = 0.006$, no overshooting). The main hydrogen burning phases are almost identical in the theoretical plane, the only difference being that the overall contraction phase begins at slightly lower T_{eff} , higher luminosity and higher age in Schaerer et al.'s track, because of the different treatments of convective borders. Again, no relevant difference is found.

4.2. Mass distribution in the upper main sequence

In order to investigate more closely the upper main sequence of the cluster, let us consider the degree of completeness of the sample under study. If we consider the stars with V between 13 and 14 mag in Vallenari et al. photometry, we find 12 stars, eight of which with a negative $(B - V)$ (Fig. 7b shows their space distribution). Among the four stars with a positive $(B - V)$, three turn out to be members of NGC 1850 main cluster (see later) and one is very likely a field red giant. We observed with *IUE* five of the hot stars, leaving out the three at the very center of NGC 1850A: these objects have magnitudes and colours very similar to those of the most luminous stars in the observed sample (V1174, V559, V562; see also data by Fischer et al. 1993, their stars 92, 97 and 101). Actually, all three appear more luminous in the visual (see Fig. 1), so that, temperatures being similar, should be more luminous also bolometrically. This means that the complete sample of stars at the tip of the main sequence is given by:

Four stars with $M \geq 55 M_{\odot}$: V1174 plus V1069, V1091, V1098

Two stars with $M \geq 40 M_{\odot}$: V559, V562

One star with $M \simeq 35 M_{\odot}$: V1115

One star with $M \simeq 20 M_{\odot}$: V1370 (giant)

We can exclude the presence of evolved massive stars (above $20 M_{\odot}$), since, with their lower temperatures, would have been brighter in the visual than V1370.

Continuing the investigation of the mass distribution along the main sequence, let us concentrate only on stars with $(B - V) < 0$, which implies, with an average reddening of 0.17 mag, to consider stars with $T_{\text{eff}} \geq 18000$ K. In the interval $14 < V < 15$, we find five objects (crosses in Fig. 7b), of which three have been observed by us: V375, V897 and V1285. Of the remaining two, one – V1037 – is similar to V1285, although slightly more luminous; the photometry of the other (V1761), located at the center of the main cluster, is probably uncertain ($V = 14.24$, close to that of V375, and $(B - V) = -0.486$). We can conclude that, in this magnitude interval, one has:

One star, possibly two, with $M \simeq 30 M_{\odot}$: V375, V1761 (?)

Three stars with $M \simeq 15 \div 20 M_{\odot}$: V897, V1285 and V1037

Again, the sample is complete also for this luminosity and the presence of evolved stars can be excluded, so that the case of V1370 appears isolated.

In the interval $15 < V < 16$, one finds 17 objects (open triangles in Fig. 7b), of which only 4 have been observed with *IUE*: V164, V381, V441 and V1336. The estimated masses vary from 12 to $17 M_{\odot}$. As an order of magnitude, these values may be assumed to be valid for all stars within this luminosity interval.

4.3. Space distribution of NGC 1850A and NGC 1850 members

Fig. 7a shows the space distribution of all the stars measured by Vallenari et al. (1994) with $V < 17$. For comparison, Fig. 7b shows only the stars with $(B - V) < 0$ and $V < 16$ mag.

Table 3. Photometric data, temperatures and luminosities for the three blue loop candidates in the main cluster NGC 1850. $E(B - V) = 0.17$ is assumed. Bolometric corrections from Kurucz (1993), for $\log g \leq 3$ (luminosity class III). Identifications as in Table 1.

Star	V	$B - V$	T_{eff}	B.C.	$\text{Log}L/L_{\odot}$
V1286	13.70	0.24	8000	-0.07	4.00
V1817	13.85	0.65	6200	-0.15	3.97
V2266	13.64	0.24	8000	-0.07	4.02

These latter stars all belong to the subcluster NGC 1850A, on the basis of their positions in the CM diagram; they have a loose distribution, apparently confined to a region west of the main cluster NGC 1850.

The situation is different when we consider stars with $(B - V) < 0$ and $V > 16$ mag, as shown in Figs. 7c–d. In particular, in the interval $16 < V < 16.3$, of the 17 stars which shows up (asterisks), about ten lie close to the main cluster center $((X, Y) = (267, 237))$, Vallenari et al. 1994), with an overall distribution neatly different from the one in Fig. 7b. We are clearly in presence of stars belonging to the main cluster NGC 1850, slightly brighter than the tip of the main sequence (see Fig. 1). Considering the objects with $16.3 < V < 16.5$ (Fig. 7d, open circles), we obtain a distribution similar to the preceding one, but more populous, that we interpret as being caused by the main sequence tip of NGC 1850. We notice also the appearance of the star group H88–159 located north–east of the main cluster (center at $(X, Y) = (370, 293))$. As pointed out earlier, the lack of stars in the southern region of the cluster is due to the presence of an arc of diffuse gas starting from H88–159 and extending toward south–west, identified by Vallenari et al.

4.4. Star V3037, the HR diagram and the age of the main cluster

The position of V3037 on the theoretical HR diagram is puzzling. In the attempt to clarify its evolutionary status, we considered in more details the CM diagram of the main cluster.

In a young cluster with a turn–off mass $\leq 40 M_{\odot}$, the most luminous stars are the helium burning giants. In the present case, the three stars with $13 < V < 14$, which lie close to the center of the main cluster, turn out to be good candidates for blue loop giants. In fact, assuming a reddening of 0.17, the inferred temperatures and luminosities (Table 3) put them on the slow section of a blue loop corresponding to an evolving mass $\leq 8 M_{\odot}$ (Fig. 6) with an age of ~ 42 Myr. At the turn–off, the estimated mass should be $\leq 7.5 M_{\odot}$, a value which is consistent with the presence of few stars above the main sequence tip, at $16 < V < 16.3$ and at a temperature of ~ 18000 K.

Star V3037 is too blue to belong to the loop of the “bona fide” helium burning giants, even using the lower T_{eff} estimate of 11500 K. It appears as a member of the group of stars falling in the Hertzsprung gap, noted by Fischer et al. (1993). Such a feature is common in the MC fields and in many MC clusters

(e.g., Garmany & Fitzpatrick 1989 and the discussion in Grebel et al. 1996).

Let us stress that the three giants just discussed are the most luminous ones of a group of seven objects (Fig. 1), which lie well above the bulk of the helium burning stars in the main cluster. So the age of the bulk of the cluster is higher than the 42 Myr mentioned before; in fact, Gilmozzi et al. (1993) find 50 ± 10 Myr, Fischer et al. (1993) 90 ± 30 Myr and Vallenari et al. (1994) $50 - 70$ Myr. An age of 50 Myr for the main cluster would be consistent with our age estimate for the brightest blue loop stars. As for the origin of these luminous (main sequence and helium burning) objects, they may be binaries or come from an episode of star formation with a delay of at least 10 Myr after the birth of the main body of the cluster.

5. Conclusions

We presented *IUE* observations of a substantial fraction of the most luminous members of the subcluster NGC 1850A. We confirm the likely presence of a variable reddening (Gilmozzi et al. 1993, Vallenari et al. 1994) with fluctuations of the order of $\Delta(E - V) \pm 0.04$; the extinction law is similar to the one observed in the 30 Doradus Nebula region.

The observed stars show an age spread of 2 to 10 Myr, with the most massive stars being the youngest. The higher age limit is strongly supported by the position of V1370, which is a giant both from the photometric and the spectroscopic point of view. The positions of lower luminosity, multiple-image objects such as V441, V1336 and V1597, even if known with good accuracy, are necessarily less conclusive.

Comparing the present age estimate with previous determinations exploiting different wavelength ranges, one finds that the cluster appears younger, the closer the wavelength range of the observations to the emission peak. In fact, Fischer et al. and Vallenari et al., with *BV* photometry find ages from 6 to 10 Myr, while Gilmozzi et al. observing in the *HST UV* bands give an age of about 4 Myr with an error of less than one Myr. As remarked by these later authors, the stellar parameters of hot stars are better defined by *UV* observations. The study in present paper makes use of spectra from 1200 to 2500 Å, with an information content higher in quantity and quality than available in preceding investigations.

In our opinion, the choice of where to perform the comparison between theoretical predictions and observations has some influence on the conclusions. We prefer to transform observational data into the theoretical H–R plane (as in Fig. 6), where it appears much easier to appreciate the position of hot, massive stars with respect to evolutionary tracks, which result almost completely degenerate in the observational plane.

The present data suggest the following age structure for NGC 1850A. Gilmozzi et al. observed with the *HST* a pre–main sequence population of stars, with mass up to $\sim 3 M_{\odot}$ and an age of about 5 Myr, if the accretion rate is $10^{-5} M_{\odot} \text{ yr}^{-1}$ (Palla & Stahler 1993). The giant V1370 ($M \sim 20 M_{\odot}$) of ~ 10 Myr may have formed in a preceding episode or, given all the uncertainties involved, may be coeval with the objects ap–

proaching the main sequence. In any case, about seven massive stars ($M \geq 35 M_{\odot}$) formed ~ 2 Myr ago, and four of these, with $M \geq 50 M_{\odot}$, formed very close to each other at what appears to be the center of NGC 1850A. Other objects with mass $\geq 20 M_{\odot}$ appear scattered between 3 and 8 Myr. On the whole, the observations support a scenario in which star formation has been active all along the lifetime of the cluster since its formation about 10 Myr ago, in a more or less constant fashion.

A similar behaviour has been suggested for other clusters and associations. Lortet & Testor (1988) studied sequential star formation processes, on a scale of 10 Myr, in stellar associations in the Magellanic Clouds. Continuous star formation over 8 – 10 Myr has been suggested for the cluster NGC 2100 (LH 111) by Hill et al. (1994), for 15 associations, about 20 Myr old, in the LMC by Kontizas et al. (1994), for NGC 1948 by Will et al. (1996), *etc.*

Admittedly, the conclusion of an age spread of 10 Myr is weakened if one considers that massive members of young clusters often belong to binary systems, may be rotating rapidly, may present an intrinsic reddening due to circumstellar disks or shells. All these factors would contribute to move the star positions in the HR diagram away from the main sequence. So estimates of rotational velocities and check of the presence of H_{α} emission, as well as theoretical tracks including the effects of rotation are badly needed to reach a safe conclusion on the matter.

If stars as young as 2 Myr are present, it becomes possible that the two supernova remnants present in the region (SNR 0509-687A and SNR 0508-688B) are physically associated with NGC 1850A (see the discussion in Vallenari et al. 1994).

As for the age of the main cluster NGC 1850, we favour an age close to the one by Gilmozzi et al. (1993), who find 50 ± 10 Myr.

Acknowledgements. Many thanks are due to Antonella Vallenari for giving us the data of the photometry of NGC 1850, to Fiorella Castelli who put at our disposal Kurucz atmospheric models, and to H.-J. Turcholke who computed for us the coordinates of reference stars in the cluster, on the basis of the Magellanic Catalogue of Stars (MACS, Turcholke et al. 1996). We thank also our referee Eva Grebel for a careful reading of the manuscript and for very helpful suggestions.

References

- Bathia R.K., MacGillivray H.T. 1987, in: M. Azzopardi and F. Matteucci (eds.), *Stellar Evolution and Dynamics in the Outer Halo of the Galaxy*, ESO Conference Workshop Proceeding No. 27, p. 489
- Bessel M.S. 1991, *A&A* 242, L17
- Brocato E., Castellani E. 1993, *ApJ* 410, 99
- Caloi V., Cassatella A., Castellani V., Walker A. 1993, *A&A* 271, 109
- Caloi V., Cassatella A. 1995, *A&A* 295, 63
- Cassatella A., Barbero J., Benvenuti P. 1985, *A&A* 144, 335
- Cassisi S., Castellani V., Straniero O. 1994, *A&A* 282, 753
- Charbonnel C., Meynet G., Maeder A., Schaller G., Schaerer D. 1993, *A&AS* 101, 415
- Feast M.W., Catchpole R.M. 1997, *MNRAS* 286, L1
- Fischer P., Welch D.L., Mateo M. 1993, *AJ* 105, 938
- Fitzpatrick E.L. 1985, *ApJ* 299, 219
- Fitzpatrick E.L. 1986, *AJ* 92, 1068
- Garmany C.D., Fitzpatrick E.L. 1989, in: K. Davidson et al. (eds.), *Physics of Luminous Blue Variables* (Kluwer, Dordrecht), p.83
- Gilmozzi R., Kinney E.K., Ewald S.P., Panagia N., Romaniello M. 1994, *ApJ* 435, L43
- Grebel E.K., Richtler T., de Boer K.S. 1992, in: B. Baschek, G. Klare, J. Lequeux (eds.), *New Aspects of Magellanic Clouds Research*, Springer Lecture Notes in Physics 416, p.366
- Grebel E.K., Roberts W.J., Brandner W. 1996, *A&A* 311, 470
- Heck A., Egret D., Jäschek M., Jäschek C. 1984, *ESA-SP* 1052
- Hill R.J., Madore B.F., Freedman W.L. 1994, *ApJ* 429, 204
- Hillebrand L.A., Massey P., Strom S.E., Merrill K.M. 1993, *AJ* 106, 1906
- Jasniewicz G., Thevenin F. 1994, *A&A* 282, 717
- Kontizas M., Kontizas E., Dapergolas A., Argyropoulos S., Bellas-Velidis Y. 1994, *A&AS* 107, 77
- Kurucz R.L. 1993, CD-ROM 13 and CD-ROM 18
- Lortet M.C., Testor G. 1988, *A&A* 194, 11
- Nandy K., Morgan D.H., Cornachan D.J. 1979, *MNRAS* 186, 431
- Oestreicher M.O., Goehermann J., Schmidt-Kaler T. 1995, *A&AS* 112, 495
- Palla F., Stahler S.W. 1993, *ApJ* 418, 414
- Panagia N., Gilmozzi R., Macchetto F., Adorf H.-M., Kirshner R.P. 1991, *ApJ* 380, L23
- Perez M.R., Huber L.F., Esper J. 1991, *IUE NASA News*. No.45, p.31
- Rountree J., Sonneborn G. 1991, *ApJ* 369, 515
- Russell S.C., Bessell M.S. 1989, *ApJS* 70, 865
- Russell S.C., Dopita M.A. 1990, *ApJS* 74, 93
- Schaerer D., Meynet G., Maeder A., Schaller G. 1993, *A&AS* 98, 523
- Schommer R.A., Geisler D. 1988 in: J.E. Grindlay and A.G. Davis Philip (eds.), *Proc. IAU Symp. No. 126, The Harlow-Shapley Symposium on Globular Cluster System in Galaxies* (Reidel, Dordrecht), p.577
- Schwering P.B.W., Israel F.P. 1991, *A&A* 246, 231
- Turcholke H.-J., de Boer K.S., Seitter W.C. 1996, *A&AS* 119, 91
- Vacca W.D., Garmany C.D., Shull J.M. 1996, *ApJ* 460, 914
- Vallenari A., Aparicio A., Fagotto F. et al. 1994, *A&A* 284 447
- van Leeuwen F., Feast M.W., Whitelock P.A., Yudin B. 1997, *MNRAS* 287, 955
- Walborn N.R., Panek R.J. 1984, *ApJ* 286, 718
- Wilcots E.M., Hodge P.W., King N. 1996, *ApJ* 458, 580
- Will J.M., Bomans D.J., Vallenari A., Schmidt J.H.K., de Boer K.S. 1996, *A&A* 315, 125
- Wu C.-C., Ake T.B., Boggess A. et al. 1983, *IUE NASA Newsl.* No. 22